Title

Surface-to-Bulk Redox Coupling through Thermally Driven Li Redistribution in Li- and Mn-Rich Layered Cathode Materials

Journal

Journal of the American Chemical Society, 141(30)

ISSN

0002-7863

Authors

Li, Shaofeng

Lee, Sang-Jun

Wang, Xuelong

et al.

Publication Date

2019-07-31

DOI

10.1021/jacs.9b05349

Peer reviewed

Surface-to-bulk redox coupling through thermally-driven Li redistribution in Li- and Mn-rich layered cathode materials

Shaofeng Li[1,2,†], Sang-Jun Lee[1,†], Xuelong Wang[3,8], Wanli Yang[4], Hai Huang[1], Daniel S. Swetz[5], William B. Doriese[5], Galen C. O'Neil[5], Joel N. Ullom[5], Charles J. Titus[6], Kent D. Irwin[6], Han-Koo Lee[1,7], Dennis Nordlund[1], Piero Pianetta[1], Chang Yu[2], Jieshan Qiu[2], Xiqian Yu[8], Xiao-Qing Yang[3], Enyuan Hu[3,*], Jun-Sik Lee[1,*], Yijin Liu[1,*]

[1]Stanford Synchrotron Radiation Lightsource, SLAC National Accelerator Laboratory, Menlo Park, CA 94025, USA

[2]State Key Lab of Fine Chemicals, School of Chemical Engineering, Liaoning Key Lab for Energy Materials and Chemical Engineering, Dalian University of Technology, Dalian 116024, China

[3]Chemistry Division, Brookhaven National Laboratory, Upton, New York 11973, USA

[4]Advanced Light Source, Lawrence Berkeley National Laboratory, 1 Cyclotron Road, Berkeley, CA 94720, USA

[5]National Institute of Standards and Technology, Boulder, Colorado 80305, USA

[6]Department of Physics, Stanford University, Stanford, California 94305, USA

[7]Pohang Accelerator Laboratory, Pohang 790-784, Republic of Korea

[8]Beijing National Laboratory for Condensed Matter Physics, Institute of Physics, Chinese Academy of Sciences, School of Physical Sciences, University of Chinese Academy of Sciences, Beijing, 100190, China

†These authors contributed equally to this work

* Correspondence and requests for materials should be addressed to E. Hu (enhu@bnl.gov), J.-S. Lee (jslee@slac.stanford.edu), or Y. Liu (liuyijin@slac.stanford.edu)

Abstract

Li- and Mn-rich (LMR) layered cathode materials have demonstrated impressive capacity and specific energy density thanks to their intertwined redox centers including transition metal cations and oxygen anions. Although tremendous efforts have been devoted to the investigation of the electrochemically-driven redox evolution in LMR cathode at ambient temperature, their behavior under a mildly elevated temperature (up to ~100 ^{o}C), with or without electrochemical driving force, remains largely unexplored. Here we show a systematic study of the thermally-driven surface-to-bulk redox coupling effect in charged $Li_{1.2}Ni_{0.15}Co_{0.1}Mn_{0.55}O_2$. We observed a charge transfer between the bulk oxygen anions and the surface transition metal cations, suggesting that the thermally-enhanced Li^+ mobility in the hosting LMR lattice could lead to significant redistribution of Li ions. Our results highlight the non-equilibrium state and dynamic nature of LMR material at deeply delithiated state and its relaxation process in response to a mild temperature perturbation.

Introduction

Lithium ion battery (LIB) technology has been widely used to power portable electronics such as laptop computers and smart phones. Recently, the worldwide interest in applying LIB for electric vehicles (EVs), has further sparked enormous research enthusiasm in this field. Considering that fossil fuels account for over 90% of the energy consumed for transportation, the projected boost in the EVs in replacing the internal combustion (IC) engine powered vehicles could have a tremendous market potential and an immense environmental impact.

The energy and power densities of the LIB are two of the most crucial properties for EV application, concerning the cruising distance and the accelerating power, respectively. To achieve the desired improvements in these properties, on the cathode side, a practical approach is to seek for addition redox center that could complement the conventional ones based solely on transition metal (TM) cations. Oxygen redox reaction, at high charging voltage, has been identified as a promising candidate and has attracted a lot of attention[1-6].

Li- and Mn-rich (LMR) layered materials have been demonstrated as a class of materials with great potential as high energy density battery cathode materials[7]. They are light, inexpensive, and well-performing. It has been demonstrated that the LMR could deliver excellent reversible capacity over 280 mAh g^{-1}. The charge compensation mechanism of LMR involves the synergistic activities of multiple redox centers[3], including the TM (Mn, Co, and Ni) cations and the oxygen anions. These redox centers are active over different voltage windows and contribute to the overall capacity differently[3]. In particular, the onset charging voltage for the oxygen redox reaction in LMR has been identified to be at over 4.5 V versus Li/Li^+ (Supplementary Fig. 1)[1, 2], highlighting oxygen anions' role at the deeply delithiated state. While oxygen anions make substantial contributions to the total capacity, they are also the origins of the notorious voltage

fade problem[8] and, thus, are currently subjected to intense studies[9-11]. Moreover, the charge transfer among different redox centers could take place in the system, further complicates the reaction mechanism.

Comparing to the amount of efforts that have been devoted into the study of the LIB cathode material's chemical evolution upon electrochemical cycling under ambient temperature, the system's redox behavior under slightly elevated temperature (up to ~100 ^{o}C) remains largely unexplored. Although the thermally-driven process is a hot research topic[12-16], the conventional wisdom holds that the mildly elevated temperature is not enough to induce significant changes. Actually, most of the reported thermally-driven electrode material degradations occur at ~200 ^{o}C and above, where the temperature is high enough to provoke mechanical disintegration[12], unwanted phase transformation[14], oxygen release[15], lithium whisker growth[13], and even thermal runaway[17-19]. These results are valuable in understanding the thermal stability of the cathode materials and safety concerns of the batteries. On the other hand, it is also very important to investigate the cathode materials under mildly elevated temperature (at ~100 ^{o}C) because such condition could occurs in liquid LIB, and is definitely required for the operation of solid-state battery with polymer electrolytes[20]. It is also critically important to the initiation of thermal runaway[18, 19]. Particularly, for the LMR cathode, the in-depth understanding of the cationic and anionic evolution under such temperature could offer profound insights into the fundamental mechanisms of the charge compensation in the system, which ultimately determines LMR materials' potential as cathode material for both conventional and solid-state LIB.

Here, we have systematically studied the thermally-driven evolution of the LMR cathode at the charged state. We have combined a set of *in-situ* probes including the X-ray imaging, X-ray diffraction, and mass spectrometry to provide complementary insights. These observations

suggest that significant lattice transformation, mechanical disintegration, and oxygen release only occurs at thermal abuse conditions at ~200 ^{o}C and above, in good agreement with the literature report[12, 13]. More thorough study of the LMR cathode's response to the mildly elevated temperature at ~100 ^{o}C, was then carried out using advanced soft X-ray spectroscopic tools including a *state-of-the-art* transition edge sensor (TES). Our results suggest that, in the bulk (probing depth at hundreds of nanometers) of the charged LMR cathode, the mild temperature elevation increase the oxidation of the O^{2-} anions but not the TM cations. To compensate for the electron release from the oxygen anions in the bulk, the TM cations (Ni, Mn, and Co) at the particle surface (probing depth up to ~10 nm) are found to have lowered valence states compared with the room temperature (RT) sample. Such surface-to-bulk redox coupling effect is likely caused by the thermally-driven lithium diffusion from the bulk to the surface, resulting in redistribution of Li ions in the LMR cathode material. Such redistribution could have profound consequences on battery operation and safety at elevated temperatures.

Results

The complicated chemomechanical interplay in charged LMR under thermal abuse conditions. For thorough investigation of the thermally-driven chemomechanical transformation in charged LMR materials, we coupled *in-situ* X-ray imaging and diffraction with mass spectrometry under controlled temperature up to 600 ^{o}C. An arbitrarily selected secondary particle, which is recovered from an LMR electrode that was harvested at the fully charged state at 4.8 V, was imaged using the X-ray nano-tomography technique (also known as transmission X-ray microscopy, TXM). As shown in Supplementary Fig. 2a, the three-dimensional (3D)

rendering and the virtual *xy*-slice through the center of the particle highlight the mesoscale morphological defects that are formed upon electrochemical cycling prior to any thermal treatments[21-25]. We present the morphological comparison between the initial state at room temperature and the state after the particle was exposed to the mildly elevated temperature at ~100 ^{o}C for ~5 hours. It appears that there no detectable changes at this scale. In contrast, further increment of the temperature to ~300 ^{o}C over the course of ~2 hours induce noticeable particle fracturing as highlighted by the two red arrows in the right panel of Supplementary Fig. 2a.

In general, the morphological degradation at the mesoscale originates from the lattice deformation which would be related with (de)intercalation of the Li ions and/or phase transformation of the hosting material. The lattice deformation leads to the buildup of mechanical stress, which is eventually released through particle cracking[26, 27]. As shown in *in-situ* X-ray diffraction (XRD) result (Supplementary Fig. 2b), the transformation of layered structure to spinel structure starts to take place at ~200 ^{o}C in the LMR sample. Further thermal abuse at even higher temperature (~450 ^{o}C) is accompanied by the transformation of spinel structure to rock salt structure. These thermally-induced phase transformations at this high temperature are also associated with the molecular oxygen release from the LMR lattice, which is clearly supported by the mass spectrometry data shown in Supplementary Fig. 2c.

Thermally-driven surface chemistry of LMR at ~100 ^{o}C. As described previously, it is of practical importance to carefully investigate the LMR materials' response to the mildly elevated temperature at up to ~100 ^{o}C. Under such condition, we did not observe any changes using the bulk sensitive *in-situ* structural probes (TXM and XRD), nor has it been reported in the literature. We, therefore, turn to studying the surface electronic structure of the charged LMR, which could have a pronounced spectroscopic fingerprint. We first carried out soft X-ray absorption

spectroscopic (XAS) measurements at all transition metals (TMs, Ni, Co and Mn) $L_{2,3}$-edges and O *K*-edge on the charged LMR electrode before and after the thermal treatment at ~100 ^{o}C for ~5 hours. As shown in Fig. 1a-c, the TMs *L*-edge XAS spectra, which were measured in the total electron yield (TEY) mode (probing depth at ~5 nm), reveal that the portion of the high valence state of TMs are relatively reduced after heating treatment. And such TM reduction is not associated with the well-known surface reconstruction phenomenon, in which the layered lattice structure reconfigures into a mixture of spinel and rock salt lattice structure. This is because the surface reconstruction is usually accompanied by the loss of oxygen from the lattice in the form of O_2 gas release and our mass spectroscopic data (Supplementary Fig. 2c) has already ruled out such possibility at 100 ^{o}C. On the other hand, the TEY signal over the oxygen K-edge remains unchanged after the thermal treatment at 100 ^{o}C. In order to maintain charge neutrality of this system, there must be a charge transfer mechanism between the bulk and the surface of the LMR material, which will be thoroughly investigated in the following sections.

The redox activity of TMs in the bulk of LMR at ~100 ^{o}C. To elucidate such surface-to-bulk redox coupling effect, we investigate the LMR's spectroscopic fingerprint via the total fluorescence yield (TFY) mode, which probes a few hundred nanometers into the bulk. Note that the TFY signal is often utilized to probe the material's bulk electronic structure. However, it suffers from the competition between the intrinsic absorption efficiency and the penetration depth, that are often going opposite at the first absorption edge very abruptly, leading to severely distorted spectrum shape. And such a distortion is further affected by the intrinsic "self-absorption" effect, which results in stronger fluorescence at higher energies than at the leading-edge energies (Supplementary Fig. 3). In particular, the TFY signal over the Mn *L*-edge are the most severely affected.

To overcome this limitation, we employed a *state-of-the-art* TES detector for measuring a partial fluorescence yield (PFY) on the LMR material. The TES detector possesses good energy resolution of ~1.4 eV over the energy range that we work with. Therefore, when equipped with a TES detector, the conventional spectroscopic scan could offer valuable insights in the resonant inelastic X-ray scattering (RIXS), PFY, and X-ray fluorescence (XRF) modalities (see Supplementary Fig. 4 for an overview of the TES-based spectroscopic data). In Fig. 2, we present the Mn, Co, and Ni $L_{2,3}$-edges RIXS data on the fully-charged LMR electrode before (left column) and after (middle column) the thermal treatment (~100 ^{o}C for ~5 hours), which shows no detectable difference. The extraction of PFY signal[28] from the regions of interest (highlighted in left and middle columns of Fig. 2) in the RIXS data greatly enhances the signal-to-noise ratio of the spectra, which carries the bulk signal of the LMR electrode. The comparison of PFY spectra (right column of Fig. 2) and the TFY spectra (Supplementary Fig. 3) clearly features the TES-facilitated data quality improvement by rejecting unwanted photons that are irrelevant to the targeted signal. This result clearly indicates that there is no significant valence state deviation of the TMs in bulk of the LMR material upon thermal treatment at ~100 ^{o}C, which is in consistent with the implication of Fig. 1. We note here that the inversed-PFY (iPFY) of the O-*K* emission signal could potentially be used to further avoid the intrinsic self-absorption induced spectrum distortion. The limited signal to noise ratio in our data is, unfortunately, insufficient for in-depth analysis of the iPFY data.

Thermally activated oxygen redox chemistry in the bulk of LMR at ~100 ^{o}C. Since the valence state of TMs in the bulk of the LMR material demonstrates no change at ~100 ^{o}C, the oxygen evolution, which has been identified as a key player in the LMR system, becomes the next focus in our search for the charge compensation mechanism for the thermally-driven surface

TMs reduction. The oxygen RIXS features have been thoroughly studied and indexed in previous literature[1, 2, 29, 30]. In particular, the oxygen RIXS feature at an excitation energy (i.e., incident photon) of ~531 eV and emission energy (emitted photon) of ~523 eV is broadly observed and is attributed to the oxygen redox activities. For LMR materials, it has been reported that the formation and evolution of this feature is associated with the deep delithiation of the LMR cathode, which activates oxygen redox reaction at high charging voltage[1]. Note that in Supplementary Fig. 5, we systematically compare the oxygen RIXS data from the LMR electrode at pristine state and fully charged state (4.8 V). We clearly observed the formation of the above mentioned RIXS feature when the LMR cathode is charged to 4.8V. Our result confirms that, at high SoC, the lattice oxygen redox reaction in LMR material is activated and is a major charge compensation mechanism for the LMR cathode at deeply delithiated state. To rule out the contamination of oxygen signal from the inactive domains in the electrode, we fabricated an electrode without loading of the active LMR particles. This LMR-free electrode has no detectable oxygen RIXS signal, confirming that the LMR is indeed the sole contributor to the measured signal of oxygen RIXS.

The comparison of the oxygen RIXS data before and after the thermal treatment of charged LMR electrode at ~100 ^{o}C (Fig. 3) suggests that the oxygen redox activity is enhanced upon heating. Such enhancement is more evident in the super-partial fluorescence yields (sPFY)[28] plots shown in Fig. 3c (see also the comparison of the normalized sPFY spectra in Supplementary Fig. 6) as well as the X-ray emission spectra at selected excitation energy (Fig. 3d-f). The temperature dependent oxygen RIXS data suggests the thermally-promoted transition of O^{2-} to oxygen with higher valence state (O^{-}) in the bulk of the LMR cathode. In other words, mildly elevated temperature could enhance the oxygen activity in the LMR lattice and, thus,

favor the oxygen redox through previously proposed mechanisms like the formation of O-O dimers[31], localized oxygen holes[9], or other specific oxygen chemical bonds[10]. The oxidation of the oxygen anions in the bulk is, therefore, the charge compensation mechanism for the reduction of TMs on the surface at ~100 ^{o}C. Such surface-to-bulk redox coupling between the TMs cations and oxygen anions are likely resulted from the thermally driven Li ions diffusion within the LMR lattice, which motivates a more thorough investigation of the lithium diffusivity in the LMR material.

Evolution of lithium diffusivity in LMR upon charging. To further understand the observed changes in the charged LMR sample upon heating to ~100 ^{o}C, it is important to investigate the influence of charging on the physical property of the LMR material, especially Li^{+} transport properties. Galvanostatic intermittent titration technique (GITT), an effective electrochemical method to calculate the lithium diffusion coefficient, is employed in this work. The experimental details are described in the method section and the analysis follows that proposed by Weppner and Huggins[32]. The GITT curve of LMR material during the 1st cycle charging is shown in Fig. 4a with the inset graph illustrating how the voltage evolves during a titration step. Specifically, upon a pulse charging, the voltage is immediately increased by IR, in which I is the current and R is the resistance, respectively. Then the voltage slowly increases, due to the galvanostatic charge pulse, in order to maintain a constant concentration gradient. When the charging current is stopped, the voltage is immediately decreased by IR. Then the voltage slowly decreases as lithium is diffused in the bulk until an equilibrium is reached in the system. By measuring various voltage increases or drops during the titration process and using the following equation, Li^{+} diffusion coefficient can be calculated[33]:

$$D_{\mathrm{Li}^+} = \frac{4}{\pi}\left(\frac{m_{\mathrm{B}}V_{\mathrm{M}}}{M_{\mathrm{B}}S}\right)^2 \left(\frac{\Delta E_{\mathrm{S}}}{\tau\left(dE_\tau \Big/ d\sqrt{\tau}\right)}\right)^2 \quad \left(\tau \ll \frac{L^2}{D_{\mathrm{Li}^+}}\right) \tag{1}$$

where m_{B} is the mass of the active material in the electrode, V_{M} is the molar volume, M_{B} is the molecular weight of LMR material, S is the active surface area of the electrode whose value is based on Brunauer, Emmett, and Teller (BET) result[34], τ is the time duration in which the current is applied, and L is the thickness of the electrode. If E_τ and τ follow a linear relationship as shown in Fig. 4b, equation (1) can be further simplified into:

$$D_{Li^+} = \frac{4}{\pi\tau}\left(\frac{m_B V_M}{M_B S}\right)^2 \left(\frac{\Delta E_S}{\Delta E_\tau}\right)^2 \tag{2}$$

The calculated lithium diffusion coefficients during 1st cycle charging of LMR material is shown in Fig. 4c. It shows that at the beginning of charging, D_{Li^+} is on the order of 10^{-14} $\mathrm{cm^2\ s^{-1}}$ which is in good agreement with results in the literature[33, 35]. When more than 0.3 Li is extracted from the lattice, a sharp decrease in D_{Li^+} is observed, with several orders of magnitude change (the y axis is $\log_{10}D_{\mathrm{Li}^+}$). A minimum in D_{Li^+} is reached (on the order of 10^{-17}) when around 0.7 Li is extracted. After that, D_{Li^+} increases but remains much lower than the initial stage of charging. Such results indicate that Li^+ transport properties deteriorates significantly in LMR material during the 1st cycle charging. This can induce a large Li concentration gradient within the particle if a relatively large current is applied for charging as in the case of normal operation. Consequently, the chemical potential of Li in the bulk is likely to be higher than that near the surface, creating thermodynamic driving force for the Li ions to migrate when the particle is relaxed. Such Li migration is believed to be the root cause of the observed surface-to bulk redox coupling phenomenon.

Discussion

Battery materials' response to elevated temperature is fundamentally important. Comparing to the tremendous amount of effort that was devoted to the investigation of battery electrodes under thermal abuse conditions, the materials' behavior at mildly elevated temperature (up to ~100 ^{o}C) is largely unexplored. One possible reason is that such mild temperature treatment can only induce very subtle if any changes, requiring highly sensitive experimental technique for detection. Also, the thermal activation of the material evolution can kinetically sluggish at such mildly elevated temperature. This temperature window, however, is relevant to several important scientific questions including the operation of solid-state battery with polymer electrolyte and the initiation of thermal runaway. These questions are of fundamental interest and substantial industrial relevance as well.

In this work, we employed a series of *in-situ* experimental techniques to investigate the charged LMR cathode's response to elevated temperature. We started with *in-situ* X-ray imaging and diffraction, together with mass spectrometry, and elucidated the structural evolution of LMR electrode at different length scales. While we clearly observe that the mesoscale particle fracturing, atomic scale lattice reconstruction, and molecular oxygen release happen concurrently at 200 ^{o}C and above, the material seems to be indifferent at temperature up to ~100 ^{o}C. We then thoroughly study the spectroscopic fingerprints of the charged LMR electrode before and after mild temperature treatment at ~100 ^{o}C for ~5 hours. We observed the reduction of TMs on the surface upon the mild thermal treatment. More importantly, the redox reaction of the lattice oxygen in the bulk of LMR material is promoted under such conditions, compensating the TM reduction on the surface. Such surface-to-bulk redox coupling effect is facilitated by the promoted lithium diffusivity at mildly elevated temperature. We further investigated the

evolution of the lithium diffusivity in LMR upon charging using GITT method, which reveals the increased resistance of lithium diffusion at high SoC. At the charged state, the LMR cathode likely exhibits a lithium concentration gradient with higher lithium concentration in the bulk and lower lithium concentration on the surface, due to the limited lithium diffusivity in LMR lattice. Starting from such ununiform distribution of lithium, the mild temperature perturbation promotes the lithium mobility and causes the system to rearrange as it settles to a new equilibrium. In this scenario, thermally-promoted ionic mobility in the hosting LMR lattice could facilitate the surface-to-bulk redox coupling effect and maximizes the entropy of the system. We have summarized our results in a schematic illustration in Fig. 5.

The presented findings and their implications offer insights into oxygen redox reaction in LMR lattice, which ultimately determines the potential of LMR material as high voltage cathode for applications in both conventional and solid-state batteries.

Methods

Electrochemical measurement. The $Li_{1.2}Ni_{0.15}Co_{0.1}Mn_{0.55}O_2$ powder was provided by Toda company. Electrodes were prepared by spreading the slurry (N-Methyl-2-pyrrolidone as the solvent) containing active materials (LMR, 80 wt.%), acetylene carbon (10 wt.%) and polyvinylidene difluoride (PVDF, 10 wt.%) as the binder and casting it on carbon-coated aluminum foils. The electrodes were then dried overnight at 120 °C in a vacuum oven and transferred into an Ar-filled glove box for future use. The active mass loadings for the electrodes were 2 mg cm^{-2}. CR2032 coin cells were assembled in an Ar-filled glovebox (O_2<0.5 ppm, H_2O<0.5 ppm) using the composite cathode, lithium foil (MTI) anode with thickness of 250 μm,

Celgard 2500 as the separator and electrolyte made of 1M LiPF6 dissolved in ethylene carbonate (EC) and ethyl methyl carbonate (EMC) (1:2 in volume). The GITT experiments were done on a Biologic SP-300 potentiostat/galvanostat. The cell was charged at a current density of 20 mA g^{-1} for 30 minutes, followed by relaxation for 4 h to reach a quasi-equilibrium state. Such process is repeated until the charging voltage limitation was reached.

***In-situ* XRD and Mass Spectroscopy.** The harvested electrode powders were loaded into a quartz tube furnace in the glove box and transferred to the thermal stage of beamline 17BM, at Advanced Photon Sources (APS), Argonne National Laboratory (ANL). The wavelength used was 0.7718 Å. To track the structural changes during thermal degradation, XRD patterns were continuously recorded by an amorphous silicon area detector (Perkin-Elmer) in the transmission mode. During heating, helium is used as the carrier gas. The outlet is connected to a mass spectrometer (i.e., residual gas analyzer, RGA) for analyzing the components of the released gas. The sample is heated from RT (25 ^{o}C) to 600 ^{o}C at a rate of 2 ^{o}C min^{-1}. Each XRD pattern takes about 3 minutes to collect. For easy comparisons with the results in the literature, the 2θ angles are converted to values corresponding to Cu Kα radiation.

***In-situ* TXM measurement.** *In-situ* nano-tomography of a selected secondary particles of the charged LMR material was carried out using the transmission X-ray microscope at beamline 6-2c at the Stanford Synchrotron Radiation Lightsource (SSRL) of the SLAC National Accelerator Laboratory. This instrument has a nominal spatial resolution of ~30 nm. More details of the experimental setup and details of the tomography reconstruction steps can be found in the literature. During the tomographic scan, the particle was rotated from -90 degree to 90 degree with a step size of 0.5 degrees. The energy was set to 9 keV for optimal zone plate efficiency and, thus, optimal signal to noise ratio. The temperature was controlled using an in-house developed

heater. Data analysis was performed using an SSRL in-house developed software package known as TXM-Wizard[36].

XAS measurement. Soft XAS measurements were carried out at the elliptically polarizing undulator (EPU) beamline 13-3 at SSRL. The two pieces of charged LMR electrode (with and without exposure to the thermal treatment at 100 ^{o}C for ~5 hours) were mounted in an ultra-high vacuum (UHV) chamber for the measurement. The vertically polarized X-ray (sigma-polarization) was used. The incident beam was monochromatized by a 600-lines/mm spherical grating monochromator (SGM), and its angle was set at 30 degrees from the sample surface. Both TFY and TEY signals were acquired simultaneously. All the XAS spectra were normalized by the intensity of the incoming X-ray beam that was concurrently measured as a drain current on an electrically isolated gold-coated mesh. A linear background, which was determined by the intensity of the pre-edge region, was subtracted from the data. Hard XAS measurements were performed at the 7-BM beamline of the National Synchrotron Light Source II (NSLS II) at Brookhaven National Laboratory (BNL) in transmission mode. The X-ray absorption near edge structure (XANES) were processed using the Athena software package[37]. The AUTOBK code was used to normalize the absorption coefficient.

RIXS measurement with TES spectrometer. RIXS measurement was performed at beamline 10-1 at the SSRL using a TES spectrometer[38, 39]. The TES spectrometer consists of a 240-channel energy-dispersive detector array facing the sample-X-ray interaction point at 90 degrees with regards to the incoming X-ray beam. The distance between the interaction point and the TES detector array was 5 cm. To achieve higher energy resolution of the TES than in a normal operation mode, only a subset of the detector array (64 pixels) was employed during the O *K*-edge RIXS measurements. In TMs *L*-edge RIXS measurements, the full detector array was used,

and each transition-metal edge was scanned 5 times (~ 550 seconds per scan), which gave sufficiently high signal-to-background ratio. The energy measured by the TES was calibrated through separate measurements of a reference sample consisting of C, N, O, and various 3d transition-metal oxides with known emission energies. Sample exposure to the air was minimized using N_2-filled glove bags during the sample mounting, and the samples were measured under UHV condition ~ $5e^{-9}$ Torr. No sign of radiation damage was observed in the RIXS measurements based on no noticeable change in the measured spectral shape between consecutive scans.

Data Availability

The data that support the plots within this paper and other finding of this study are available from the corresponding author upon reasonable request.

Acknowledgments

Use of the Stanford Synchrotron Radiation Lightsource, SLAC National Accelerator Laboratory, is supported by the U.S. Department of Energy (DOE), Office of Science, Office of Basic Energy Sciences under Contract No. DE-AC02-76SF00515. The work done at Brookhaven National Laboratory was supported by the Assistant Secretary for Energy Efficiency and Renewable Energy, Vehicle Technology Office of the U.S. Department of Energy through the Advanced Battery Materials Research (BMR) Program, including Battery500 Consortium under contract DE-SC0012704. This research used beamline 7-BM of the National Synchrotron Light Source II, a U.S. Department of Energy (DOE) Office of Science User Facility operated for the

DOE Office of Science by Brookhaven National Laboratory under Contract No. DE-SC0012704. This research used beamline 17BM of the Advanced Photon Source, a U.S. Department of Energy Office of Science User Facility operated for the DOE Office of Science by Argonne National Laboratory under Contract No. DE-AC02-06CH11357. The engineering support from D. Van Campen, D. Day and V. Borzenets for the TXM experiment at beamline 6-2C of SSRL is gratefully acknowledged.

Author contributions

Y. Liu, J.-S. Lee, and E. Hu conceived the study. X. Wang, E. Hu, and X. Yu prepared the battery electrode and carried out electrochemical testing including GITT measurement. S. Li, S.-J. Lee, H. Huang, J.-S. Lee, Y. Liu performed synchrotron RIXS experiments and data processing. S. Li, E. Hu, J.-S. Lee, and Y. Liu wrote the manuscript with valuable input from all coauthors. S.-J. Lee, D. Swetz, W.B. Doriese, G.C. O'Neil, J. Ullom, C.J. Titus, K.D. Irwin, and D. Nordlund contributed to the development and deployment of the TES spectrometer at SSRL. W. Yang, P. Pianetta, C. Yu, J. Qiu, X. Yu and X.-Q. Yang contributed to the interpretation of the data. S. Li and S.-J. Lee contributed equally to this work.

Competing financial interests

The authors declare no conflicts of interest.

References

1. Gent, W.E. et al. Coupling between oxygen redox and cation migration explains unusual electrochemistry in lithium-rich layered oxides. *Nat. Commun.* **8**, 2091 (2017).
2. Xu, J. et al. Elucidating anionic oxygen activity in lithium-rich layered oxides. *Nat. Commun.* **9**, 947 (2018).
3. Hu, E. et al. Evolution of redox couples in Li- and Mn-rich cathode materials and mitigation of voltage fade by reducing oxygen release. *Nat. Energy* **3**, 690-698 (2018).
4. Assat, G. & Tarascon, J.-M. Fundamental understanding and practical challenges of anionic redox activity in Li-ion batteries. *Nat. Energy* **3**, 373-386 (2018).
5. Xie, Y., Saubanère, M. & Doublet, M.L. Requirements for reversible extra-capacity in Li-rich layered oxides for Li-ion batteries. *Energy Environ. Sci.* **10**, 266-274 (2017).
6. Sathiya, M. et al. Reversible anionic redox chemistry in high-capacity layered-oxide electrodes. *Nat. Mater.* **12**, 827-835 (2013).
7. Yang, F. et al. Nanoscale morphological and chemical changes of high voltage lithium-manganese rich NMC composite cathodes with cycling. *Nano Lett.* **14**, 4334-4341 (2014).
8. Croy, J.R., Balasubramanian, M., Gallagher, K.G. & Burrell, A.K. Review of the U.S. department of energy's "deep five" effort to understand voltage fade in Li- and Mn-rich cathodes. *Acc. Chem. Res.* **48**, 2813-2821 (2015).
9. Luo, K. et al. Charge-compensation in 3d-transition-metal-oxide intercalation cathodes through the generation of localized electron holes on oxygen. *Nat. Chem.* **8**, 684-691 (2016).
10. Seo, D.-H. et al. The structural and chemical origin of the oxygen redox activity in layered and cation-disordered Li-excess cathode materials. *Nat. Chem.* **8**, 692-697 (2016).
11. Maitra, U. et al. Oxygen redox chemistry without excess alkali-metal ions in $Na_{2/3}[Mg_{0.28}Mn_{0.72}]O_2$. *Nat. Chem.* **10**, 288-295 (2018).
12. Yan, P. et al. Coupling of electrochemically triggered thermal and mechanical effects to aggravate failure in a layered cathode. *Nat. Commun.* **9**, 2437 (2018).
13. Wei, C. et al. Thermally driven mesoscale chemomechanical interplay in $Li_{0.5}Ni_{0.6}Mn_{0.2}Co_{0.2}O_2$ cathode materials. *J. Mater. Chem. A* **6**, 23055-23061 (2018).
14. Mu, L. et al. Propagation topography of redox phase transformations in heterogeneous layered oxide cathode materials. *Nat. Commun.* **9**, 2810 (2018).
15. Mu, L. et al. Oxygen release induced chemomechanical breakdown of layered cathode materials. *Nano Lett.* **18**, 3241-3249 (2018).
16. Hu, E. et al. Utilizing environmental friendly iron as a substitution element in spinel structured cathode materials for safer high energy lithium-ion batteries. *Adv. Energy Mater.* **6**, 1501662 (2016).
17. Finegan, D.P. et al. In-operando high-speed tomography of lithium-ion batteries during thermal runaway. *Nat. Commun.* **6**, 6924 (2015).
18. Finegan, D.P. et al. Characterising thermal runaway within lithium-ion cells by inducing and monitoring internal short circuits. *Energy Environ. Sci.* **10**, 1377-1388 (2017).
19. Finegan, D.P. et al. Identifying the cause of rupture of Li-ion batteries during thermal runaway. *Adv. Sci.* **5**, 1700369 (2018).
20. Besli, M.M. et al. Mesoscale chemomechanical interplay of the $LiNi_{0.8}Co_{0.15}Al_{0.05}O_2$ cathode in solid-state polymer batteries. *Chem. Mater.* **31**, 491-501 (2019).
21. Mao, Y. et al. High-voltage charging-induced strain, heterogeneity, and micro-cracks in secondary particles of a nickel-rich layered cathode material. *Adv. Funct. Mater.* **29**, 1900247 (2019).

22. Wei, C. et al. Mesoscale battery science: the behavior of electrode particles caught on a multispectral X-ray camera. *Acc. Chem. Res.* **51**, 2484-2492 (2018).
23. Liu, H. et al. Intergranular cracking as a major cause of long-term capacity fading of layered cathodes. *Nano Lett.* **17**, 3452-3457 (2017).
24. Tsai, P.-C. et al. Single-particle measurements of electrochemical kinetics in NMC and NCA cathodes for Li-ion batteries. *Energy Environ. Sci.* **11**, 860-871 (2018).
25. Wang, J., Chen-Wiegart, Y.-c.K. & Wang, J. In situ three-dimensional synchrotron X-ray nanotomography of the (de)lithiation processes in tin anodes. *Angew. Chem. Int. Ed.* **53**, 4460-4464 (2014).
26. Xu, R., de Vasconcelos, L.S., Shi, J., Li, J. & Zhao, K. Disintegration of meatball electrodes for $LiNi_xMn_yCo_zO_2$ cathode materials. *Exp. Mech.* **58**, 549-559 (2018).
27. Xia, S. et al. Chemomechanical interplay of layered cathode materials undergoing fast charging in lithium batteries. *Nano Energy* **53**, 753-762 (2018).
28. Dai, K. et al. High reversibility of lattice oxygen redox quantified by direct bulk probes of both anionic and cationic redox reactions. *Joule* **3**, 518-541 (2019).
29. Wu, J. et al. Fingerprint oxygen redox reactions in batteries through high-efficiency mapping of resonant inelastic X-ray scattering. *Condens. Matter* **4**, 5 (2019).
30. Yang, W. & Devereaux, T.P. Anionic and cationic redox and interfaces in batteries: advances from soft X-ray absorption spectroscopy to resonant inelastic scattering. *J. Power Sources* **389**, 188-197 (2018).
31. McCalla, E. et al. Visualization of O-O peroxo-like dimers in high-capacity layered oxides for Li-ion batteries. *Science* **350**, 1516-1521 (2015).
32. Weppner, W. & Huggins, R.A. Determination of the kinetic parameters of mixed conducting electrodes and application to the system Li_3Sb. *J. Electrochem. Soc.* **124**, 1569-1578 (1977).
33. Li, Z. et al. Electrochemical kinetics of the $Li[Li_{0.23}Co_{0.3}Mn_{0.47}]O_2$ cathode material studied by GITT and EIS. *J. Phys. Chem. C* **114**, 22751-22757 (2010).
34. Nanda, J., Martha, S.K. & Kalyanaraman, R. High-capacity electrode materials for electrochemical energy storage: role of nanoscale effects. *Pramana* **84**, 1073-1086 (2015).
35. Yu, H. et al. Electrochemical kinetics of the $0.5Li_2MnO_3 \cdot 0.5LiMn_{0.42}Ni_{0.42}Co_{0.16}O_2$ 'composite' layered cathode material for lithium-ion batteries. *RSC Adv.* **2**, 8797-8807 (2012).
36. Liu, Y. et al. TXM-Wizard: a program for advanced data collection and evaluation in full-field transmission X-ray microscopy. *J. Synchrotron Rad.* **19**, 281-287 (2012).
37. Ravel, B. & Newville, M. ATHENA, ARTEMIS, HEPHAESTUS: data analysis for X-ray absorption spectroscopy using IFEFFIT. *J. Synchrotron Rad.* **12**, 537-541 (2005).
38. Titus, C.J. et al. L-edge spectroscopy of dilute, radiation-sensitive systems using a transition-edge-sensor array. *J. Chem. Phys.* **147**, 214201 (2017).
39. Doriese, W.B. et al. A practical superconducting-microcalorimeter X-ray spectrometer for beamline and laboratory science. *Rev. Sci. Instrum.* **88**, 053108 (2017).

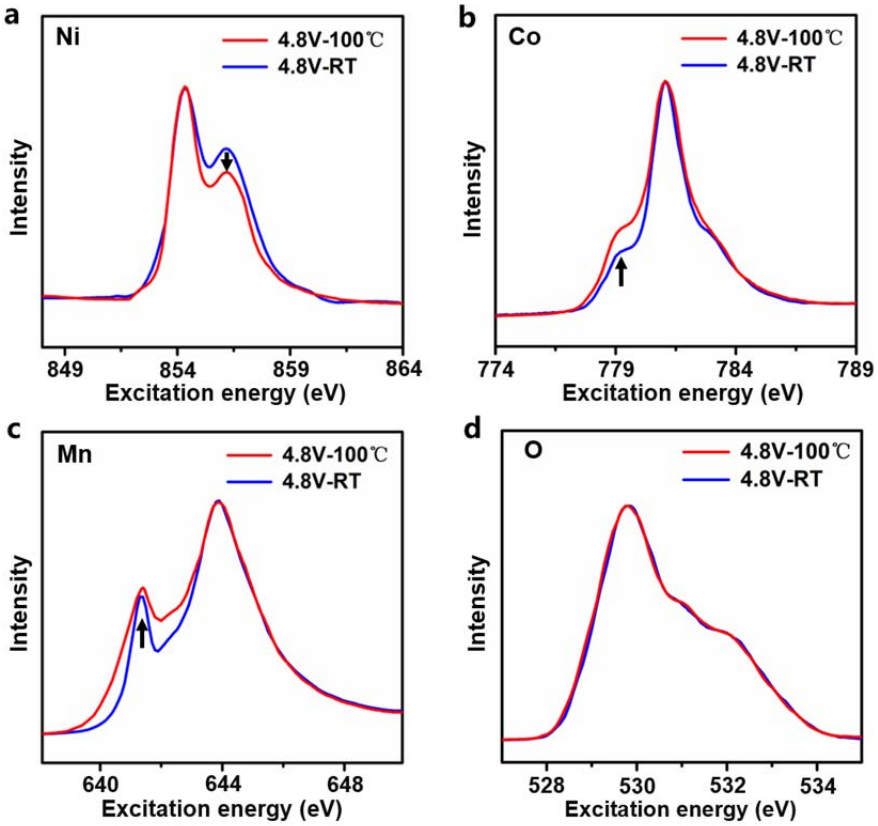

Fig. 1 TEY signals from the charged (4.8 V) LMR electrode before and after it is exposed to mildly elevated temperature (100 ^{o}C) for ~5 hours. The transition metal elements (Ni, Co, and Mn) appear to be slightly reduced upon heating. All the spectra were normalized at the maximum.

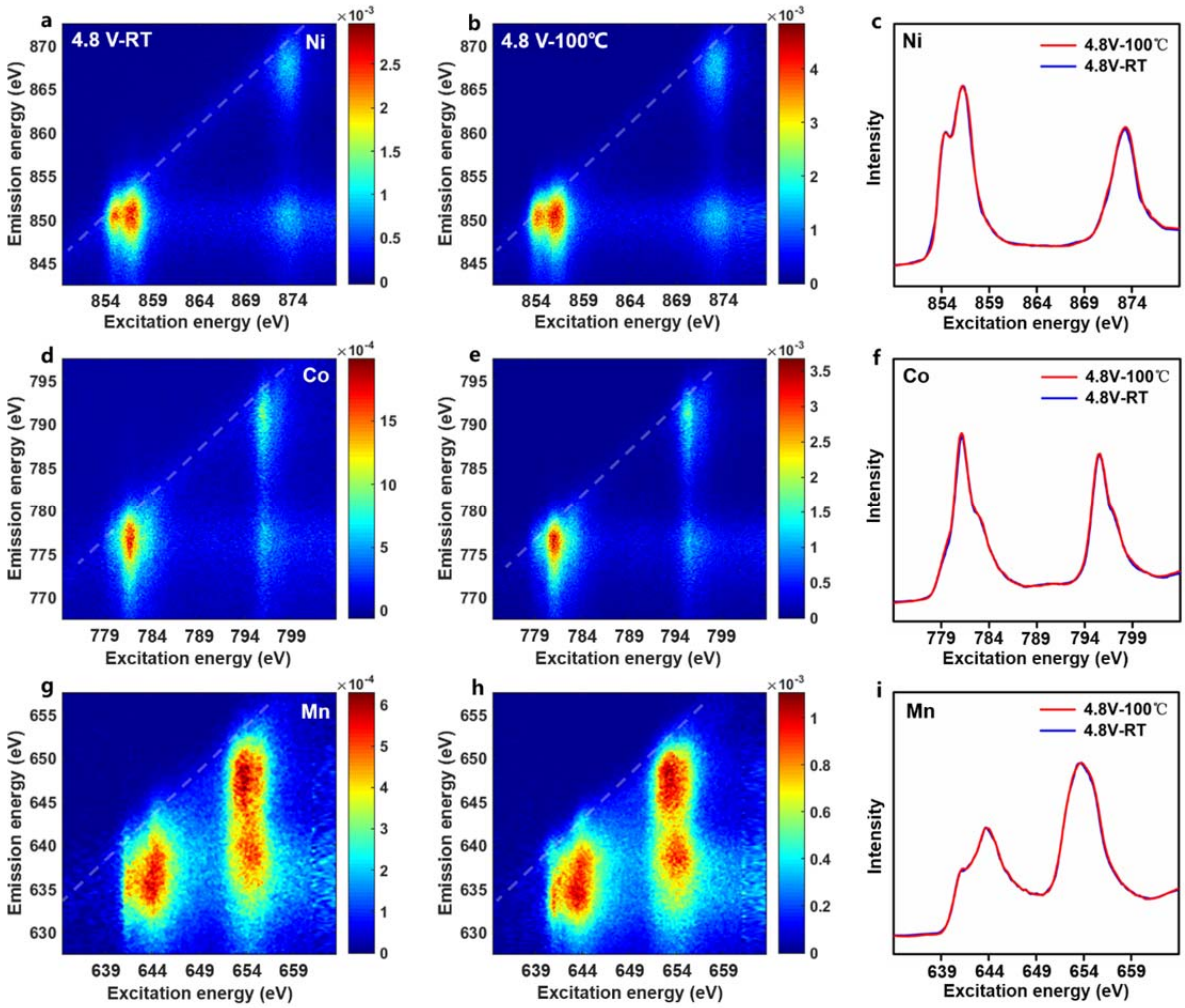

Fig. 2 RIXS (left and middle column) and PFY (right column) fingerprints of transition metal elements (Ni (a-c), Co (d-f), and Mn (g-i)) in fully-charged (4.8 V) LMR electrode before and after the thermal treatment at ~100 ^{o}C for ~5 hours. Panels (a), (d) and (g) are the RIXS maps collected on the charged LMR electrode under room temperature. Panels (b), (e), and (h) are the RIXS maps collected after the thermal treatment. Panels (c), (f), and (i) are the comparison of PFY signals before and after the thermal treatment. The PFY spectrum is extracted by vertically integrating the signal in corresponding RIXS map. The diagonal white dashed lines in all the RIXS maps are ascribed to the elastic line. No noticeable thermally-induced changes are observed in the RIXS and PFY signatures over the transition metal elements' absorption *L*-edges.

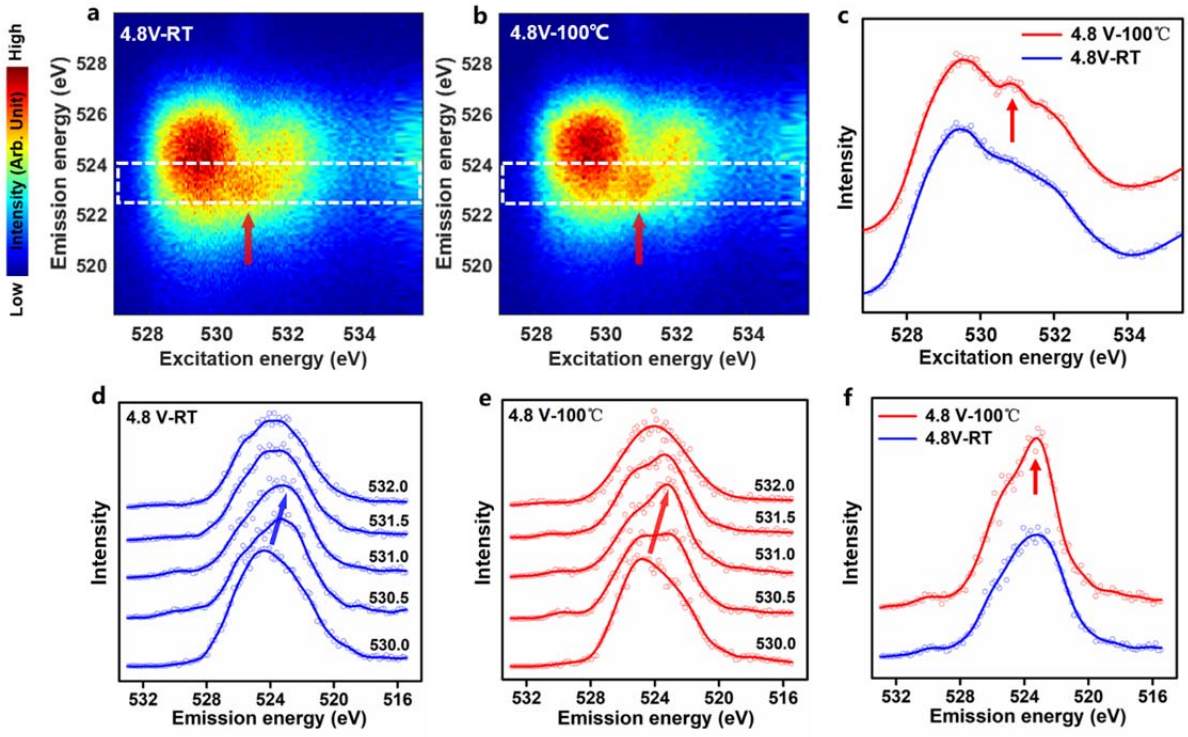

Fig. 3 Oxygen RIXS maps from the charged LMR electrode at room temperature (panel (a)) and after thermal treatment at ~100 ^{o}C for 5 hours (panel (b)). Panel (c) is the sPFY signal extracted by vertically integrating the signal across a super-partial range marked by the white frames in panels (a) and (b). Panels (d) and (e) are the X-ray emission spectra at selected excitation energy points from 530 eV to 532 eV in RIXS maps (a) and (b), respectively. Panel (f) is the comparison of the X-ray emission spectra at excitation energy of 531 eV shown in Panel (d) and (e). The formation and enhancement of the RIXS feature at excitation energy of ~531 eV and emission energy of ~523 eV, which is attributed to the oxygen redox reaction, are clearly observed. The solid lines are guide to eyes.

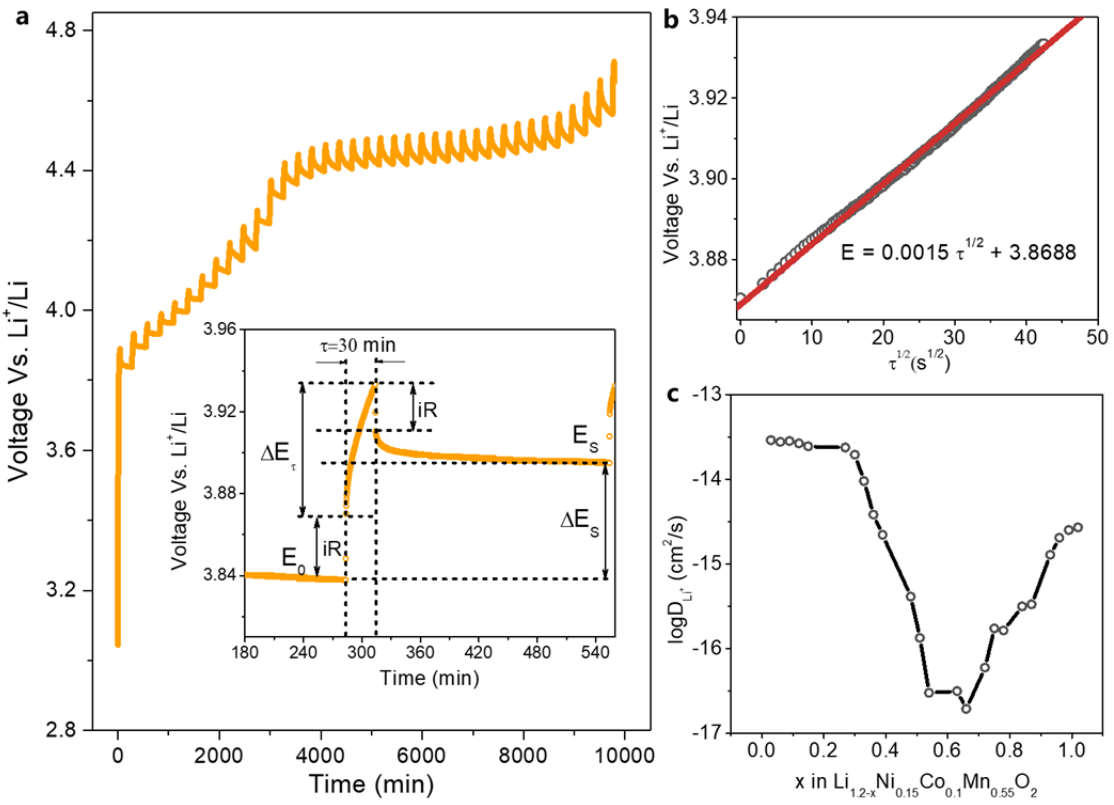

Fig. 4 GITT measurement of LMR and the computed lithium diffusivity during charging. (a) Voltage profile during the GITT experiment with the inset graph showing how voltage evolves during a titration step. The meanings of the variables are described in the text. (b) The linear relationship between voltage and the square root of τ during the voltage increase stage when the current is applied. (c) Li ion diffusivity evolution during the first cycle charging process of LMR material.

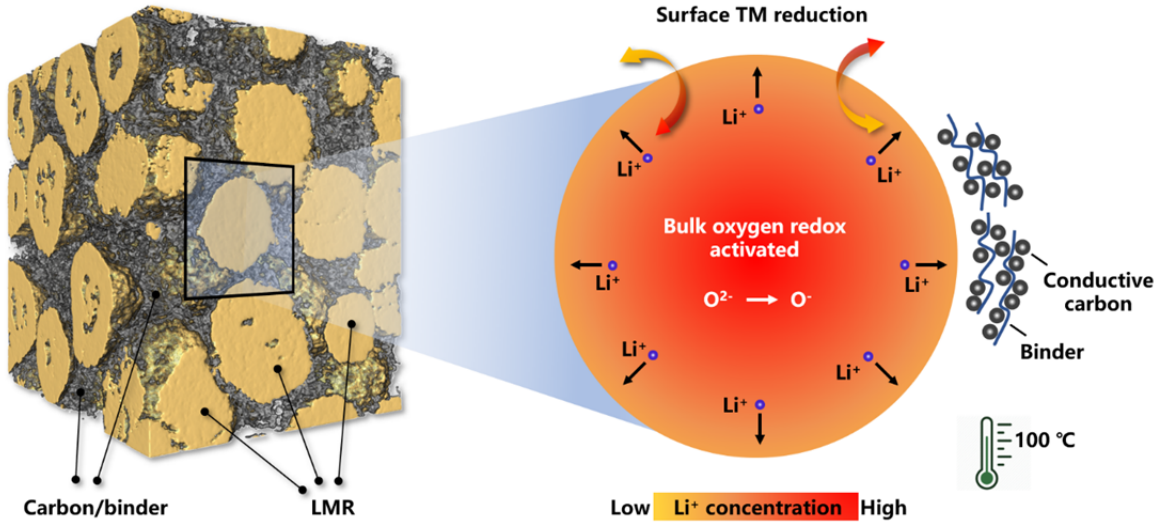

Fig. 5 Schematic illustration of the observed thermally activated redox coupling effect. The mild temperature elevation to 100 ^{o}C triggers the charge transfer between the oxygen anions in the bulk and the transition metal cations on the particle surface through activation of the lithium ion diffusion.